Optical Materials 96 (2019) 109362

Contents lists available at ScienceDirect

Optical Materials

journal homepage: www.elsevier.com/locate/optmat

Study of charge carrier trapping by EPR and TSL methods in $Zn_xMg_{1-x}WO_4$ single crystals

N. Krutyak[a,*], D. Spassky[b], V. Nagirnyi[c], M. Buryi[d], I. Tupitsyna[e,f], A. Dubovik[e,f]

[a] Physics Department, Moscow State University, Leninskie Gory 1(2), 119991, Moscow, Russia
[b] Skobeltsyn Institute of Nuclear Physics, Moscow State University, Leninskie Gory 1(2), 119991, Moscow, Russia
[c] Institute of Physics, University of Tartu, W. Ostwald str. 1, 50411, Tartu, Estonia
[d] Institute of Physics AS CR, Cukrovarnicka 10, 162 00, Prague, Czech Republic
[e] Institute for Scintillation Materials, NAS of Ukraine, 60 Nauky Ave., 61072, Kharkiv, Ukraine
[f] V. N. Karazin Kharkiv National University, 4 Svobody Sq, 61022, Kharkiv, Ukraine

ARTICLE INFO

Keywords:
Zinc tungstate
Magnesium tungstate
Mixed crystals
Charge carrier trapping
EPR
TSL

ABSTRACT

Charge carrier trapping was studied using EPR and TSL methods in $ZnWO_4$, $MgWO_4$ and mixed $Zn_xMg_{1-x}WO_4$ crystals. An electron trapped at a perturbed W site was detected in $MgWO_4$. It was also shown that holes are trapped at oxygen ions thus forming O^- centers. Two different O^- centers, one perturbed by a cation vacancy, another by Al impurity, were found in $MgWO_4$, while a single hole center perturbed by Cd impurity and hydroxyl group nearby was detected in $ZnWO_4$. The number of non-equivalent hole centers increases up to five for the mixed crystals due to the perturbations induced by statistically distributed substitutional cations. It is shown that the thermal release of holes is accompanied by thermostimulated luminescence (TSL). The broadening of the TSL peaks typically observed in mixed crystals is connected with the increase of the number of non-equivalent trapping centers of the same type.

1. Introduction

Zinc and magnesium tungstates are promising scintillating materials for application in rare events search experiments [1,2]. Recently an enhancement of the light output has been detected in $Zn_xMg_{1-x}WO_4$ mixed bulk and nanocrystals compared to that of their constituents $ZnWO_4$ and $MgWO_4$ [3,4]. The light output of mixed bulk and nanocrystals increases up to 150% and 450%, respectively, compared to that of $ZnWO_4$. The structural and optical characteristics of mixed compounds demonstrate linear dependence on x, while the efficiency of energy transfer to luminescence centers increases for the intermediate values of x, reaching the highest value for x = 0.5 [5]. The effect is ascribed to the disorder in the sublattice of substitutional cations that results in the confinement of the charge carrier thermalization length and serves as a key factor for the observed light yield enhancement [6]. The trapping of charge carries is also supposed to be influenced by substitutional cations disorder. It is known that the peaks of thermostimulated luminescence in mixed crystals are broader than in their constituents [7–9]. To understand the reason of the TSL peak broadening, we used the EPR method as the most straightforward technique which allows to determine the origin of the defects responsible for charge carriers trapping. Here, we present the results of the study of trapping centers in $ZnWO_4$ and $MgWO_4$ crystals, as well as their modification in $Zn_xMg_{1-x}WO_4$ mixed crystals, using the combination of TSL and EPR methods.

2. Experimental details

The single crystals of $Zn_xMg_{1-x}WO_4$ (x = 0, 0.3, 0.4, 0.5, 0.6, 0.8, 1) were grown by the Czochralski technique from platinum crucibles using high-frequency heating. The single crystal of $MgWO_4$ was grown from melted flux solution by pulling on a rotating seed from a platinum crucible. Solid-phase synthesis method was used to obtain the charge for the single crystal growth. Initial oxides for the charge were ZnO (99.995%), MgO (99.95%) and WO_3 (99.995%). The flux was prepared from Na_2WO_4 (99.95%). All the grown crystals belong to the wolframite structural type.

EPR measurements were carried out on a Bruker X-/Q-band E580 FT/CW ELEXSYS spectrometer at X-band (9.4 GHz). The temperature region was 30–296 K. The magnetic field sweep range was chosen rather narrow to study irradiation-induced centers with the aim to intensify observed signals by increasing scan time. Temperature for a

* Corresponding author.
E-mail address: krutyakn@yahoo.com (N. Krutyak).

https://doi.org/10.1016/j.optmat.2019.109362
Received 26 April 2019; Received in revised form 27 August 2019; Accepted 4 September 2019

single measurement was selected in most cases such as to avoid saturation and find the best signal-to-noise ratio. Samples were X-ray irradiated at liquid nitrogen temperature using an ISO-DEBYEFLEX 3003 highly stabilized X-Ray equipment for structure analysis (tungsten X-ray tube, 55 kV, 30 mA). All procedures of EPR spectra fitting were performed using the "Easyspin 5.0.0 toolbox" program [10]. Tungstate crystal samples were not oriented and thus all EPR measurements were done in an arbitrary orientation of the samples with respect to an external magnetic field. For this reason all fitting parameters were omitted in the text below as they did not provide any physically useful information.

TSL glow curves were obtained using a CRYOTRADE LN-120 cryostat equipped with a LakeShore 335 temperature controller. Samples were UV-irradiated for 30 min at 77 K and then heated to 270 K with a linear rate 10 K/min. TSL curves were recorded using an H7732-11 photosensor module. The luminescence excitation spectra of the samples were measured using a 150 W Xe lamp as an excitation source while luminescence signal was detected using an Oriel MS 257 spectrograph equipped with a Marconi CCD detector.

Absorption and reflection spectra were measured using a PerkinElmer Lambda 950 spectrophotometer. The measurements of absorption spectra were performed in the temperature range 77–500 K using a CRYOTRADE LN-120 cryostat.

3. Results and discussion

3.1. EPR studies of $Zn_xMg_{1-x}WO_4$ single crystals

The lattice symmetry of tungstates studied in the present work belongs to the P2/c space group, wolframite type. It allows seven structurally equivalent and non-equivalent sub-lattices, each of which can offer a paramagnetic impurity ion one or two magnetically non-equivalent positions in the lattice [11]. EPR spectra measured in such samples will show, respectively, either one or two similar signals, split due to the magnetically inequivalent positions and dependent on the site occupied. However, if the materials are contaminated, the impurities can break the local symmetry and thus increase the number of certain sites at least twice, so that instead of one or two lines, two or four can be observed [11]. Exactly the same situation will be discussed below.

The EPR spectra of non-irradiated $ZnWO_4$ and $MgWO_4$ samples exhibited the traces of some accidental paramagnetic impurities (Fig. 1). Gd^{3+} revealed itself in the fine and hyperfine structures (HFS)

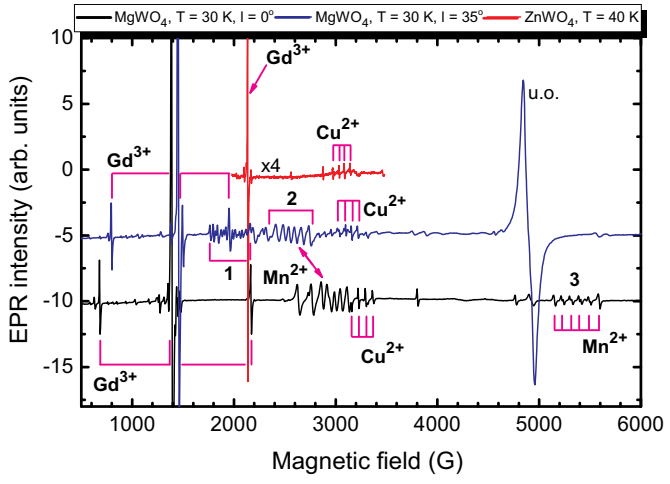

Fig. 1. EPR spectra measured in $MgWO_4$ and $ZnWO_4$ before X-ray irradiation. "u.o." assigns the resonance line of unknown origin. The spectra produced by Cu^{2+} and Mn^{2+} ions are stressed. "1–3" numbers indicate visible Mn^{2+} transitions.

characteristic for an ion with electron spin S = 7/2, studied in detail in $ZnWO_4$:Gd [12]. The HFS arises because of the ^{155}Gd and ^{157}Gd nuclei with non-zero nuclear magnetic moment, i.e. with the nuclear spin I = 3/2 with 15% and 16% abundance, respectively. Mn^{2+} was found due to the peculiar fine structure (transitions "1–3" in Fig. 1) and sextet of lines with pronounced and specifically spaced HFS (~90 G) [13–17]. Cu^{2+} ($3d^9$) was identified due to a characteristic spectrum studied in $CdWO_4$, $MgWO_4$ and $ZnWO_4$ [18]. The Cu^{2+} impurity occupies most probably one position, since only one very specific quartet of lines (HFS from ^{63}Cu and ^{65}Cu, both having nuclear spin I = 3/2 and 69% and 31% natural abundance, respectively) was detected. No other similar signals were found in the spectra, which would allow to refer to another kind of Cu^{2+} ion. At the same orientation, a broad and strong line, obviously composed of several poorly resolved components, appears in the spectrum of $MgWO_4$ ("u.o." in Fig. 1). Its origin remains unknown. No EPR signals coming from impurity centers other than Gd^{3+} ions were detected in the non-irradiated $Zn_xMg_{1-x}WO_4$ mixed crystals. Most probably the detected impurities originate from initial materials used for crystal synthesis and some of them perhaps were induced from a crucible in the process of crystal growth. It is noteworthy, that X-ray irradiation did not affect the corresponding EPR lines, allowing a conclusion that the detected impurities are stable and do not facilitate radiation defect creation in their closest surrounding.

X-ray irradiated samples show the creation of various paramagnetic centers. In $ZnWO_4$ and mixed tungstates, all the observed irradiation-induced centers were hole-like O^- defects ($2p^5$ outer shell). All were characterized by g factors slightly higher than the free electron value 2.0023 and the spectral positions of the EPR lines were slightly dependent on sample orientation with respect to an external magnetic field direction, having this in common with the O^- defects described in other materials [19–27]. In $MgWO_4$, beside the O^- defect, an electron-like center was detected as well. The principal view of the corresponding EPR spectra did not significantly depend on x in the 0.2–0.8 range in the mixed crystals, except slight variations in thermal stability (~10 K) of the respective irradiation-induced centers. This result obviously coming from small perturbations in the local surrounding as the Zn^{2+} ions in $ZnWO_4$ and Mg^{2+} ions in $MgWO_4$ have almost the same ionic radii in octahedral environment, i.e. 0.74 Å and 0.72 Å, respectively [28].

EPR spectra of irradiated $MgWO_4$ are shown in Fig. 2. Since the crystal sample was not oriented, they have been taken at an arbitrary orientation of the external magnetic field with respect to the crystal axes. Two different types of centers, electron-like and hole-like, were detected. The hole-like type is represented by two distinct centers labelled as O^-(I) and O^-(II). The EPR signal of the second one exhibits a pronounced superhyperfine structure (SHFS, see an inset in Fig. 2). It is composed of six equally spaced resonance lines of the same intensity with some weaker satellites beside. This suggests hyperfine interaction of the paramagnetic electron with a nucleus presented in the majority (more than 50%) by the isotope with the nuclear spin I = 5/2 of a non-paramagnetic ion. There are several stable elements possessing such property: ^{27}Al (100% natural abundance); ^{55}Mn (100% natural abundance); ^{185}Re and ^{187}Re, 37.4% and 62.6% natural abundance, respectively, both having I = 5/2; ^{121}Sb (I = 5/2, 57.2% abundance), and ^{123}Sb (I = 5/2, 32.8% abundance); ^{141}Pr, 100% abundance. Manganese, rhenium and praseodymium may be excluded because the hole trapping might occur at their ions directly. It has been shown, for example, in $Li_2B_4O_7$ [29] that X-rays cause the decrease of the total Mn^{2+} EPR intensity supposing thus a hole capture and Mn^{3+} creation. The Mn^{2+} signal measured in $MgWO_4$ does not lose its intensity upon the X-ray irradiation. $Sb^{3+,5+}$ are also expected to trap holes [30]. Moreover, referring to the purity of the starting materials for the crystals synthesis given in Ref. [3], no antimony, praseodymium and rhenium ions could be expected in the samples studied. On the other hand, Al^{3+} cannot take part in a direct hole trapping processes. Besides, electron and hole traps associated with the Al^{3+} impurity have been already studied in

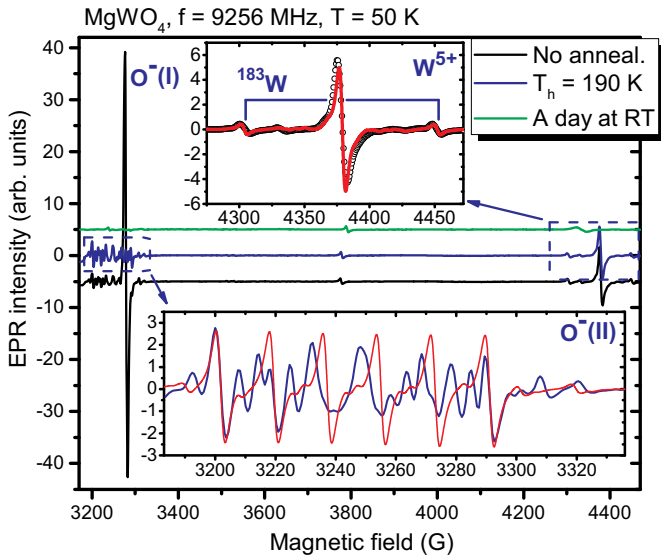

Fig. 2. Experimental EPR spectra (solid lines) of the O^-(I), O^-(II) and W^{5+} irradiation-induced centers in $MgWO_4$ measured at an arbitrary orientation of an external magnetic field with respect to the crystal axes. The W^{5+} signal exhibits clearly resolved hyperfine structure due to the ^{183}W intrinsic nucleus as indicated in the upper inset. Another two spectra measured before annealing ("No anneal.") and after heating of the sample up to T_h = 190 K are demonstrated. O^-(II) spectrum is shown zoomed in a lower inset. Simulated spectra are provided in red. (For interpretation of the references to colour in this figure legend, the reader is referred to the Web version of this article.)

$ZnWO_4$ [31]. Therefore, one may rather expect a hole trapped at an oxygen ion and stabilized by an Al^{3+} ion nearby. The super hyperfine interaction in the O^-(II) experimental spectrum (a lower inset in Fig. 2) was fitted by the calculated one by using the following spin-Hamiltonian:

$$\widehat{H} = \beta_e g_{eff} S_z B + S_z A(Al) I_z(Al) + S_z A(W) I_z(W) + S_z A(Mg) I_z(Mg), \quad (1)$$

where g_{eff}, β_e are the effective g factor and the Bohr magneton; S_z, B are the electron spin operator ($S = 1/2$) and magnetic field, respectively; $A(Al)$ is SHF tensor of ^{27}Al, $I_z(Al)$ is the corresponding nuclear spin operator. Similar designations are given for tungsten and magnesium nuclei. It can be seen that, the simulation gives a satisfactory agreement with the experiment. Some deviations originate from an arbitrary orientation of a crystal, so additional splitting of the lines may occur, which due to the low ^{25}Mg and ^{183}W abundances, approximately 10% and 14%, respectively, can hardly be resolved. Besides, the forbidden transitions were not considered. The parameters of fit were: $g_{eff} = 2.08 \pm 0.01$, $A(^{27}Al) = 52 \pm 2$ MHz, $A(^{183}W) = 168 \pm 8$ MHz, $A(^{25}Mg) = 60 \pm 8$ MHz. Remarkably, the ^{27}Al superhyperfine constant is approximately twice as large as that reported for W^{5+} in Ref. [31]. Unfortunately, for the Al-related hole trap in $MgWO_4$ the superhyperfine interaction with the aluminum nucleus was very weak (the nucleus was too far from the center) to be determined. Similarly to the case of $ZnWO_4$ [31] the Al^{3+} ion was expected to substitute for Mg^{2+}. According to the $MgWO_4$ crystal structure [32], only the O2 type of the possible distinct oxygen positions (O1 and O2) is connected to two Mg ions. Based on this analysis, the O^-(II) center can be described as O2 + Al + W + Mg. The proposed center model is shown in Fig. 3a.

The O^-(I) center is different. It is characterized by a single line accompanied by obscure satellites. Moreover, its spectrum is strongly overlapped with that of the O^-(II) when the crystal is rotated in an arbitrary plane. Therefore, one may expect it to originate from a similar lattice site, e.g., O1 [28], which, however, in contrast to O^-(II) is most probably not perturbed by an imperfection nearby. The analysis of the

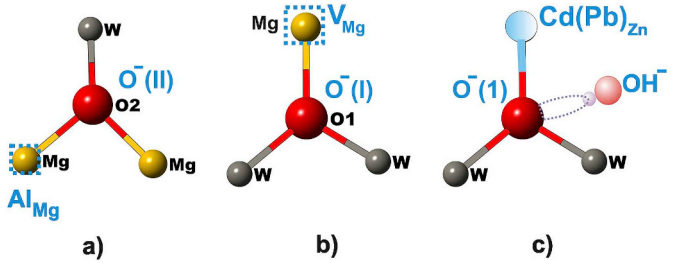

Fig. 3. Irradiation-induced center models. a) $MgWO_4$, O^-(II) – O2 + W + Mg + Al_{Mg}, b) $MgWO_4$, O^-(I) – O1 + 2W + V_{Mg}, c) $ZnWO_4$, O^-(1) – O2 + 2W + Cd_{Zn} (first coordination sphere within 3 Å radius) and OH^- are shown.

SHFS of the O^-(I) spectra in the similar way like it was described above, shows a possible contribution from two equivalent tungsten nuclei. They can be observed at orientations different from that in Fig. 2, but these satellite transitions are so strongly overlapped with the central line that a quantitative analysis would be rather speculative. However, the hyperfine constant was estimated to be about 15 MHz for each tungsten nucleus. It is approximately 10 times lower than for the O^-(II) discussed above. The structure due to ^{25}Mg is completely indiscernible in the O^-(I) SHFS. The centers O^-(I) and O^-(II) have different thermal stability. The O^-(I) center disappears already after heating up to 190 K while the spectrum of O^-(II) survives unchanged as it is shown in Fig. 2. Therefore, it was impossible to estimate the SHFS unambiguously basing on the presented data. All these considerations lead to the following center model: O1 + 2W + V_{Mg} (Fig. 3b). Magnesium vacancy then could be responsible for the shift of O^- towards it and consequent reduction of the hyperfine interaction with two tungsten nuclei as compared to the O^-(II) center.

Therefore, one may expect that both trapped holes constituting O^-(I) and O^-(II) centers are rather defect-related than self-trapped. Remarkably, self-trapped holes have been detected in the isostructural $ZnWO_4$ earlier [25], however, it seems that holes can be trapped next to some defects as well. For instance, O^- defect affected by Li was observed in $ZnWO_4$:Li [33]. It is known that self-trapped holes or electrons exhibit very low thermal stability [21]. In the present case, X-rays irradiation was delivered to the samples at 77 K which is probably too high temperature for the self-trapping processes to be observed.

The electron-like center has g factor lower than 2.0023. In particular, the corresponding signal shown in Fig. 2 is observed at $g = 1.54$. It was deduced to be related to the W^{5+} ion, due to a pronounced hyperfine structure of the ^{183}W nucleus clearly observed. The experimental spectrum was fitted with the calculated one by using the following spin-Hamiltonian:

$$\widehat{H} = \beta_e g_{eff} S_z B + S_z A(W) I_z(W) + \sum_{i=1}^{2} S_z A(Mg_i) I_z(Mg_i), \quad (2)$$

where contributions of two slightly different magnesium nuclei were taken into account beside the tungsten one. The fit parameters were: $g_{eff} = 1.54 \pm 0.01$, $A(^{183}W) = 317 \pm 8$ MHz, $A(^{25}Mg_1) = 72 \pm 2$ MHz, $A(^{25}Mg_2) = 64 \pm 8$ MHz. The calculated spectrum is in good agreement with the experimental one shown in the upper inset in Fig. 2. Large ^{183}W hyperfine constant along with the g factor smaller than 2.0023 presents evidences for the electron center to be W^{5+}. Different hyperfine constants of the $^{25}Mg_1$ and $^{25}Mg_2$ nuclei suggest local perturbations of the centers, influencing their thermal stability as it is shown further. Besides W is a structural component of the material and a transition ion which can be easily recharged [34–36]. Moreover, the effective g factor and ^{183}W hyperfine constant demonstrate values common for the W^{5+} ion, if compared, for example, with such charge trap detected in isostructural $ZnWO_4$ [31,37–39].

In $ZnWO_4$, only one hole-like O^- center was found. The

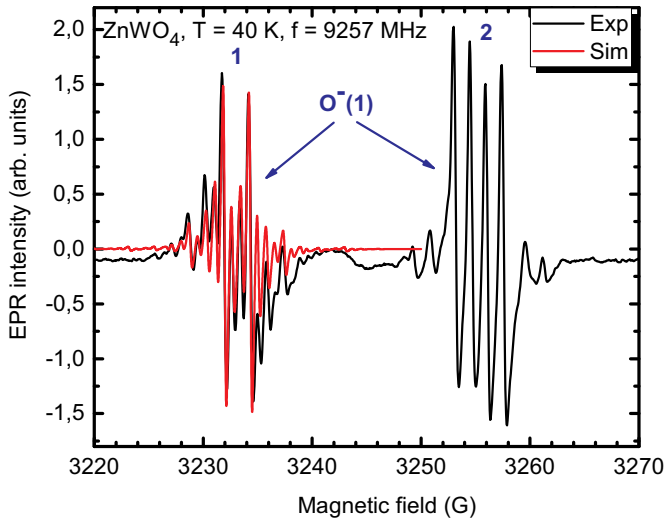

Fig. 4. EPR spectrum of O^-(1) center in $ZnWO_4$. Two components "1" and "2" originate from the same center but at two magnetically inequivalent positions. The component "1" was fitted by the simulated spectrum.

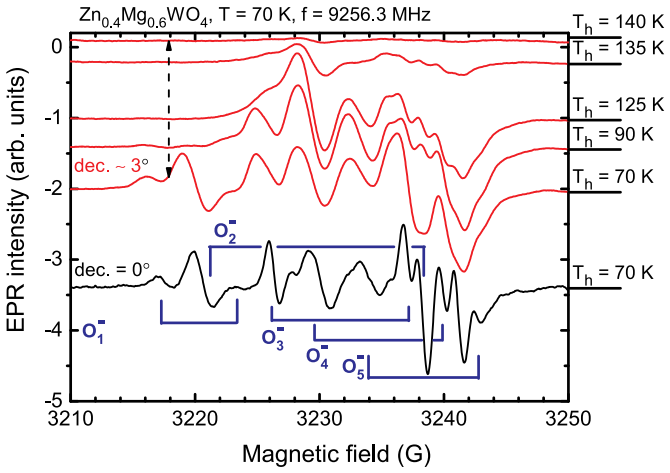

Fig. 5. EPR spectra measured from the $Zn_{0.4}Mg_{0.6}WO_4$ crystal (T = 70 K, f = 9256.3 MHz). "dec." accounts for the declination angle in an arbitrary sample rotation plane so the spectrum with the dec. = 0° is eventually the initial one. The ~3° difference (see "dec. ~3°" spectra) appears due to an irregular sample (not oriented) shape. The "0°" and "~3°" spectra were measured separately. The spectra are also distinguished by the annealing temperature T_h.

corresponding spectrum consisting of the components "1" and "2" is shown in Fig. 4. Both components demonstrate the same intensity dependence on annealing temperature (see Fig. 7) according to thermal stability study (described in detail below). Some small difference may come out of occasional temperature shift in EPR measurements. The components are attributed to the same paramagnetic center which occupies a site allowing at least two magnetically inequivalent positions. However, according to Ref. [11] the $ZnWO_4$ lattice does not possess such site. Thus, a local distortion occurring, most likely, due to additional tensions in the nearest surrounding of the site can be anticipated. To have a clearer image of the trapping center origin, the component "1" of the O^- spectrum (labelled O^-(1) by analogy with centers in $MgWO_4$) was analyzed similarly to the O^-(II) in $MgWO_4$ (see Fig. 2). The experimental spectrum 1 in Fig. 4 was approximated by the calculated one assuming the interaction of a paramagnetic electron with surrounding nuclei as follows: O2 + OH^- + (2W + Cd $(Pb)_{Zn})_{r1}$ + (2Zn + 2W)$_{r2}$ (oxygen lattice site is given in accordance with [40]). Here, r1 = 3 Å and r2 = 4 Å are radii-vectors of the first and second coordination spheres containing the nuclei listed in the parentheses, which contribute to the super hyperfine structure in the spectra in Fig. 4. Note that the interaction with a hydrogen nucleus in a hydroxyl was also taken into account. For example, the O^- - V_{Zn} – OH^- trapping center has been described in $ZnWO_4$ previously [31]. The spin-Hamiltonian similar to the ones in Eqs. (1) and (2) was used taking into account superhyperfine interactions with H, W, Cd, Pb and Zn nuclei as introduced above. The fit parameters were: g_{eff} = 2.0457 ± 0.0002; $A(H_{OH})$ = 7 ± 2 MHz; $A(W_{r1})$ = 9 ± 2 MHZ; $A(W_{r2})$ = 4 ± 2 MHz; $A(Cd(Pb)_{r1})$ = 18 ± 2 MHz; $A(Zn_{r2})$ = 10 ± 2 MHz. It should be noted that the obtained values of effective g factor and hydrogen hyperfine constant are similar to those for the O^- - V_{Zn} – OH^- center [31]. As one can see, the calculated spectrum demonstrates almost perfect agreement with the experimental one. The Zn^{2+} ion from the first coordination sphere should be replaced by the Pb^{2+} or Cd^{2+} ion (both having isotopes with nuclear spin I = 1/2 and natural abundance about 20%), however, Cd^{2+} ion is more probable since $CdWO_4$ [41] is nearly isostructural to $ZnWO_4$. No other combination of nuclear contributions could give even nearly as good fit. The cadmium ion can be the source of above-mentioned tensions which lead to the creation of two magnetically inequivalent positions of the same oxygen site. Thus, the discovered center is perturbed and cannot be regarded a self-trapped hole. The proposed center model is shown in Fig. 3c where only the first coordination sphere and hydroxyl group are taken into account since the second one is supposed to undergo no or much smaller perturbations.

In the mixed tungstates, five hole-like O^- defects were found. The corresponding spectra marked O^-_{1-5} are shown for $Zn_{0.4}Mg_{0.6}WO_4$ in Fig. 5. Despite the strong mixing of resonance lines it was possible to roughly resolve the signals coming from different O^- centers, characterized by different thermal stability, by carrying out measurements at 70 K after the annealing steps indicated in Fig. 5. Due to poor resolution it was impossible to distinguish SHFS and, consequently, to deduce the origin of the centers. However, one may suggest them to be located at either O1 or O2 anion regular lattice sites (Fig. 3a and b) [32,40] with differently perturbed local surroundings due to the alternating Zn and Mg in the lattice.

In order to demonstrate the relation between the O^- defect centers and thermally stimulated luminescence we studied the conditions of defect creation under UV radiation and analyzed the correlations between the thermal stability of defect centers and features in TSL curves.

3.2. TSL excitation spectra of $Zn_xMg_{1-x}WO_4$ single crystals

An O^- defect center is created when a hole is trapped at an oxygen ion. To create separated electrons and holes the energy of an exciting photon has to be sufficiently high. In the EPR experiment, the crystals were irradiated using a high-energy X-ray source. For the TSL experiments, we used a UV light source and performed the studies aimed at the determination of the creation threshold of separated charge carriers in studied crystals. Usually the threshold corresponds to the bandgap value E_g in undoped crystals, however in some cases, it can exceed E_g due to the features of the band structure and phenomena related to the mobility threshold [42,43].

The intrinsic luminescence of $ZnWO_4$, $MgWO_4$ and $Zn_xMg_{1-x}WO_4$ is connected with the radiative annihilation of excitons self-trapped at the WO_6 complexes [3,44,45]. It can be excited starting from the fundamental absorption edge of the crystals (see Fig. 6, panels (a), curves 2 and absorption spectra in panels (b)), that is typical for the emission centers of intrinsic origin. The excitation spectra of TSL are presented in Fig. 6, panels (a), curves 1. The lowest energy E_{e-h} needed to create separated electrons and holes, deduced from the threshold of the TSL signal observation, was 4.58, 4.76 and 4.95 eV for $ZnWO_4$, $Zn_{0.4}Mg_{0.6}WO_4$ and $MgWO_4$, respectively. The E_{e-h} value increases in mixed crystals gradually from $ZnWO_4$ to $MgWO_4$, which is connected with gradual increase of the bandgap with the increase of Mg content [5]. It is worth noting that previous estimations of E_{e-h} in $ZnWO_4$

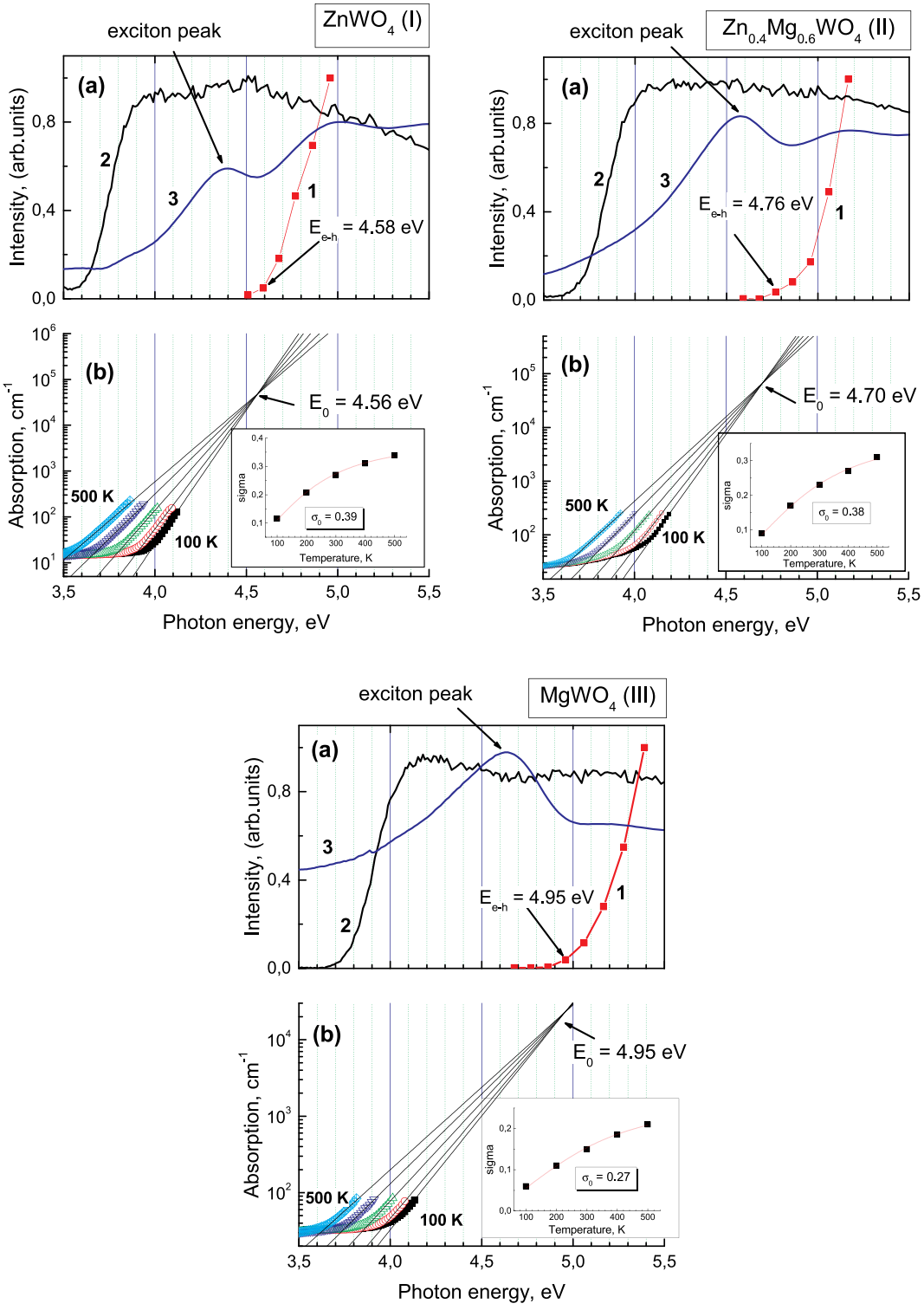

Fig. 6. (a) TSL excitation (1), luminescence excitation (2) and reflection (3) spectra for $ZnWO_4$ (I), $Zn_{0.4}Mg_{0.6}WO_4$ (II) and $MgWO_4$ (III). Curves 1 were measured for TSL peaks in 80–200 K range, curves 2 and 3 were measured at 300 K. (b) Energy dependences of the absorption coefficient measured at 100, 200, 300, 400 and 500 K are represented by dots. Sample thickness was 0.1 mm for $ZnWO_4$ and $Zn_{0.4}Mg_{0.6}WO_4$ and 0.3 mm for $MgWO_4$. The lines represent the fit of eq. (1)Eq 3 to the experimental data. In the inset: temperature dependence of the steepness parameter σ (squares) and it's fit by Eq 4 (line).

performed using photo-stimulated luminescence excitation method gave higher values than obtained in the present study [45,46]. The discrepancy may be connected with lower sensitivity of luminescence registration or with peculiarities of the photo-stimulated method used for the estimation of $E_{e\text{-}h}$ in previous studies.

The threshold of TSL excitation spectra is shifted by 1.0–1.2 eV to higher energies with respect to that of luminescence excitation spectra. At $E < E_{e\text{-}h}$ the steady luminescence is excited via direct creation of excitons, while separated electrons and holes are not created. In order to prove this supposition, we have performed a fit of temperature dependence of the absorption coefficient. The absorption coefficient is an exponential function of the photon energy in the region of the

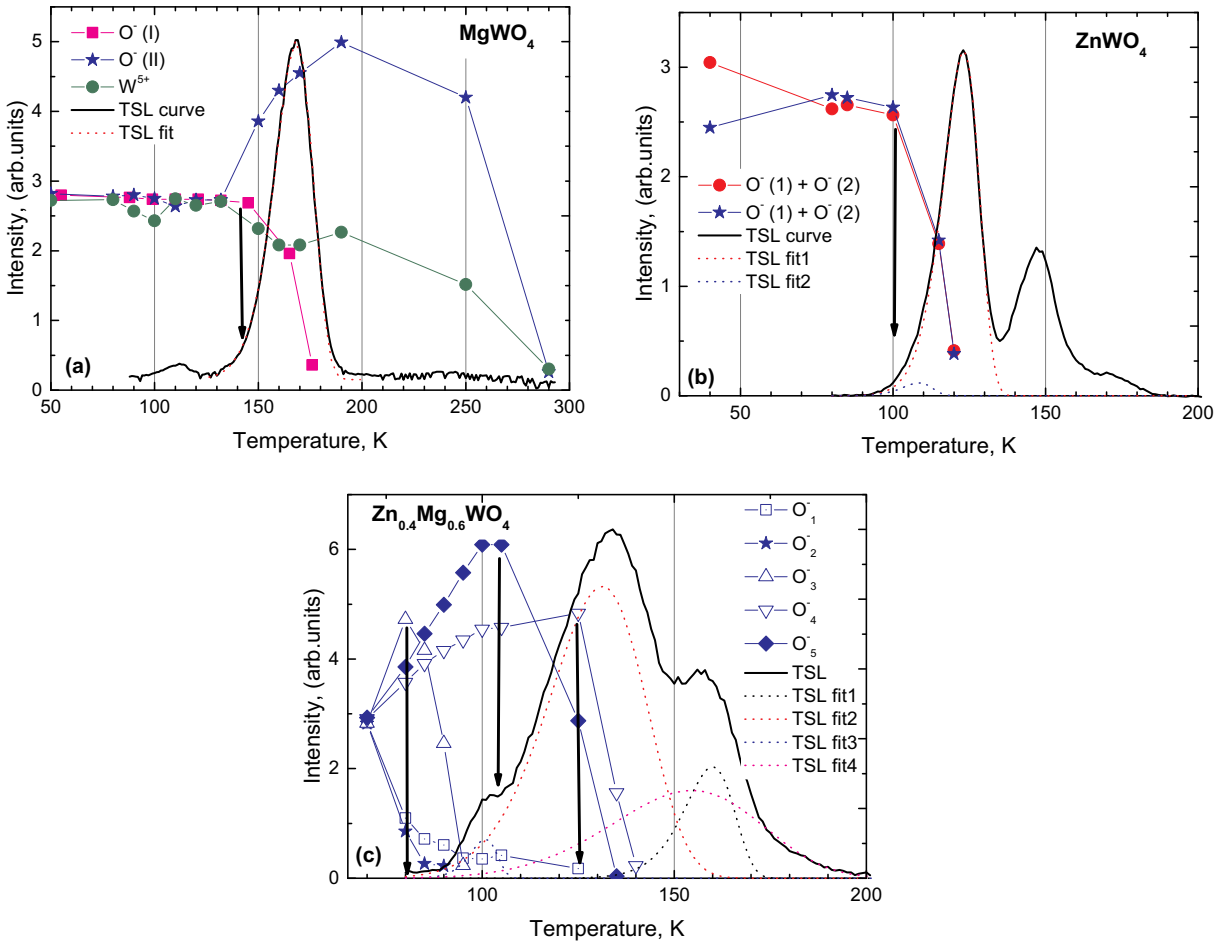

Fig. 7. TSL curves and temperature dependence of EPR intensity of all the irradiation-induced centers for $MgWO_4$ (a), $ZnWO_4$ (b) and $Zn_{0.4}Mg_{0.6}WO_4$ (c) crystals.

fundamental absorption edge (the so-called Urbach tail). This dependence can be described by the following formula [47]:

$$\alpha(h\omega) = \alpha_0 \exp\left(-\sigma\frac{E_0 - E}{k_B T}\right), \quad (3)$$

where α_0 and E_0 are the characteristic coordinates for the given compound of the intersection point of the extended Urbach edges at different temperatures, k_B is the Boltzmann constant and T is temperature, σ is the temperature-dependent steepness parameter which can be represented as:

$$\sigma(T) = \sigma_0 \frac{2kT}{\hbar\omega_p}\tanh\left(\frac{\hbar\omega_p}{2kT}\right), \quad (4)$$

where $\hbar\omega_p$ is an average energy of the interacting phonons and σ_0 is the limit of σ at high temperatures.

The fit of Equation (3) to the experimental data is presented in Fig. 6, panels (b). The extrapolation of the fitting lines for different temperatures intersect at a point $\alpha_0 \sim 10^4$ - 10^5 cm^{-1} and E_0 = 4.56, 4.70 and 4.95 eV for $ZnWO_4$, $Zn_{0.4}Mg_{0.6}WO_4$ and $MgWO_4$, respectively. The value of E_0 corresponds usually to the energy of an exciton peak in a given compound [48]. The obtained E_0 values are slightly lower than that of $E_{e\text{-}h}$. As $E_{e\text{-}h}$ corresponds to the bandgap and E_0 to the energy of exciton peak, the observed difference arises due to the binding energy of excitons. The obtained values of E_0 are in relatively good correspondence to the position of the first reflectivity peak (Fig. 6, panels (a), curves 3) which has been previously shown to be of excitonic origin [49]. The position of exciton reflectivity peak depends on temperature and its maximum shifts to higher energies with temperature decrease thus approaching the E_0 value.

The value of σ_0 was calculated using formula (4) (see inset in Fig. 6, panels (b)). The σ_0 parameter characterizes the strength of the exciton–phonon interaction and allows to predict whether the self-trapping of excitons is expected in a given compound. The value of σ_0 below unity is a criterion for exciton self-trapping, otherwise the creation of free excitons could be expected. The obtained σ_0 values are small and similar for all studied crystals (0.39, 0.38, and 0.27 for $ZnWO_4$, $Zn_{0.4}Mg_{0.6}WO_4$, and $MgWO_4$, respectively), thus confirming a strong exciton-phonon interaction and exciton self-trapping in these crystals.

It also worth noting that even at energies below $E_{e\text{-}h}$ we have observed a weak TSL signal which can probably be explained by recharging effects in defect pairs.

3.3. Thermal stability of trap centers and TSL curves

Thermal stability of the centers found in $ZnWO_4$, $Zn_{0.4}Mg_{0.6}WO_4$ and $MgWO_4$ was studied by the pulse annealing method. The samples were annealed up to certain temperature, kept at this temperature for 3 min and quickly cooled down to the reference temperature of 40 K at which the EPR spectrum was measured. The cycle was repeated continuously, each time increasing the annealing temperature, until the EPR signal disappeared completely. The dependence of the EPR intensity on heating temperature is shown for various centers in Fig. 7 together with TSL curves. The TSL curves were obtained after irradiation of the samples by photons with energy E_{ex} = 5.5 eV for 30 min at 77 K.

The EPR signal intensity of the O^-(I) center decreases starting from T_h = 140 K in $MgWO_4$ (Fig. 7a). The holes released in this process are partially recaptured at the deeper O^-(II) centers, the number of which reaches its maximum at T_h = 195 K. In the same temperature range, some part of the holes recombines with electrons trapped at the W^{5+} centers, causing a decrease of their number. The TSL curve for $MgWO_4$ is characterized by the presence of an intense peak at 170 K. Its rise at ~140 K coincides with the threshold of thermal release of holes from the O^-(I) centers (arrow in Fig. 7a). Thus, the TSL peak can be attributed to the recombination of holes released from O^-(I) center with electrons trapped at W^{5+} center. The experimental TSL curve was perfectly fitted by a single peak with E_{act} = 0.25 eV and frequency factor $\omega_0 = 6 \times 10^5$ cm^{-1} in the first order kinetic approximation [20,50].

Upon the increasing annealing temperature over 200 K one can observe another recombination process, leading to a complete depletion of O^-(II) hole centers and W^{5+} electron traps at approximately 290 K. Unlike the case of the above-described recombination of O^-(I) related holes with W^{5+} centers, no TSL peak was detected in this temperature region. In view of the fact that the crystal photoemission is not quenched at these temperatures, one can only suggest an opposite sign of the reaction, namely, a thermal release of electrons from W^{5+} traps and their non-radiative recombination with O^-(II) hole centers. Considering a relatively high temperature at which this processes takes place, the W^{5+} center cannot be regarded as a self-trapped electron observed in some tungstates and molybdates at much lower temperatures [20,35,36].

One also can note a slight decrease of the concentration of trapped electrons at T = 80–100 K, which is accompanied by a weak TSL peak at 112 K. However, the concentration of trapped electrons returns to its initial value at 110 K, while the concentration of holes trapped at O^-(I) and O^-(II) centers does not change. Therefore, there is no direct correlation between the TSL peak at 112 K and the change in the concentration of trapped charge carriers. The variations of EPR signal amplitude in this temperature range can be ascribed to fluctuations during the measurements.

In $ZnWO_4$, the O^-(1) signal remains almost unchanged until the annealing at 100 K and then reduces steeply by 120 K. The rise of the TSL peak coincides with the threshold of thermal release of holes from the O^-(1) EPR centers at T > 100 K (arrow in Fig. 7b). Fitting the TSL peak at 123 K by a single curve in the first order kinetics approximation was unsuccessful. It can be fitted by the superposition of at least two peaks (E_{act}^1 = 0.21 eV, $\omega_0^1 = 10^7$ cm^{-1}, E_{act}^2 = 0.19 eV, $\omega_0^2 = 5 \times 10^7$ cm^{-1}) which correspond to thermal release of holes from two different centers. The EPR analysis has shown that the O^-(1) center is characterized by two components "1" and "2", which originate from two magnetically inequivalent positions of the center. Thus, this TSL peak can be attributed to the recombination of holes released from both inequivalent positions of the EPR center. In contrast to $MgWO_4$, the TSL curve of $ZnWO_4$ consists of two pronounced peaks. The second TSL peak at 147 K is caused by thermal release of charge carriers from non-paramagnetic centers.

The data on thermal stability of hole centers in the $Zn_{0.4}Mg_{0.6}WO_4$ mixed crystal are presented in Fig. 7c. The $O^-_{1,2}$ centers are characterized by very low stability and are thermally destructed already at 90 K. Self-trapped holes are not observed in the investigated crystals because they are released at lower temperatures than the temperature of crystal irradiation. It is known, that this process occurs at 50 K in $ZnWO_4$ [25,45,51] and $MgWO_4$ [52]. Some part of the holes released from the $O^-_{1,2}$centers is re-trapped by deeper traps. In particular, the EPR intensity of the O^-_3 center rises at approximately 90 K with consequent fast destruction at 95 K. The remaining two hole traps O^-_4 and O^-_5 recapture the holes from the depleted $O^-_{1,2}$, which is confirmed by the increase of the intensity of the corresponding EPR signals from 90 to 115 K. Both centers disappear completely at about 140 K, although the thermal stability of the O^-_4 is a bit higher. Both hole centers are obviously stabilized by some defect or impurity nearby.

The TSL curve of $Zn_{0.4}Mg_{0.6}WO_4$ is complicated with a pronounced maximum at 134 K and satellite peaks at 102 and 157 K, which is in the temperature region where TSL peaks are observed in $ZnWO_4$ and $MgWO_4$ single crystals. The TSL curve can be fitted by a superposition of four peaks (E_{act}^1 = 0.33 eV, $\omega_0^1 = 5 \times 10^9$ cm^{-1}, E_{act}^2 = 0.11 eV, $\omega_0^2 = 120$ cm^{-1}, E_{act}^3 = 0.24 eV, $\omega_0^3 = 5 \times 10^{11}$ cm^{-1}, E_{act}^4 = 0.09 eV, $\omega_0^4 = 5$ cm^{-1}). The peaks can be attributed to the thermal decay of the O^-_{1-5} hole centers. The annihilation of the O^-_2 center starts at 70 K that is below the low-temperature limit of TSL registration and the center is completely destroyed at 85 K. Therefore, this center did not contribute to the formation of the TSL curve. The release of holes from other four centers results in the appearance of four TSL peaks. The thermal release of the holes from the O^-_3 centers results in the intensive TSL peak at ~100 K with E_{act}^3 = 0.24 eV. The disintegration of the O^-_1 and O^-_5 centers is prolonged in temperature scale. The thermal release of the former center starts at 70 K and occurs in two steps with its complete disintegration at 125 K. The corresponding values for the O^-_5 center are 105 K and 135 K, respectively. We suppose that broad peaks with E_{act}^2 = 0.11 eV and E_{act}^4 = 0.09 eV arise due to the disintegration of these centers. Finally, thermal disintegration of the O^-_4 centers starts at 125 K and is accompanied by the rise of the high-temperature TSL peak with maximum at 157 K and E_{act}^1 = 0.33 eV.

Structural disorder, which arises due to cationic substitution in mixed crystals results in the increase of the number of capture centers of the same origin in comparison to that in their constituents. The detection of five different O^- EPR centers in the case of $Zn_{0.4}Mg_{0.6}WO_4$ mixed crystal instead of two such centers in $ZnWO_4$ confirms this conclusion. The increase of the number of trapping centers results in the broadening of TSL peaks, which is usually observed for mixed crystals [7–9].

4. Conclusions

$ZnWO_4$ and $MgWO_4$ single crystals as well as $Zn_{0.4}Mg_{0.6}WO_4$ mixed crystal were studied using EPR and TSL techniques. EPR analysis reveals the creation of the variety of defect centers in the studied crystals after X-ray irradiation at low temperatures. It is shown that the main defects in these crystals may be categorized as hole-like O^- centers. Two types of the O^- centers, one with Al impurity and the other with Mg vacancy nearby, were detected in $MgWO_4$. One type of the O^- centers perturbed by a cadmium ion and hydroxyl group was detected in $ZnWO_4$. Up to five O^- defects were found in the $Zn_{0.4}Mg_{0.6}WO_4$ mixed crystal, which originate from differently perturbed local surroundings due to the partial disorder of crystal structure. It is shown that the thermal release of trapped holes results in the appearance of TSL peaks. The broadening of TSL peaks, which is usually observed in the mixed crystals, is connected with the increase of the number of non-equivalent trapping centers of the same origin.

Declaration of competing interest

The authors declare that they have no known competing financial interests or personal relationships that could have appeared to influence the work reported in this paper.

Acknowledgements

The authors gratefully acknowledge the financial support of the Ministry of Education, Youth and Sports of Czech Republic, projects LO1409 and CZ.02.1.01/0.0/0.0/16_013/0001406, Estonian Research Council (project PUT PRG111) and ERDF funding in Estonia granted to the Centre of Excellence TK141 (Project No. 2014-2020.4.01.15-0011).

References

[1] P. Belli, R. Bernabei, F. Cappella, et al., Final results of an experiment to search for 2β processes in zinc and tungsten with the help of radiopure $ZnWO_4$ crystal scintillators, J. Phys. G Nucl. Part. Phys. 38 (1–15) (2011) 115107.

[2] P. Belli, A. Incicchitti, F. Cappella, Inorganic scintillators in direct dark matter investigation, Int. J. Mod. Phys. A 29 (1–44) (2014) 1443011.

[3] D. Spassky, S. Omelkov, H. Magi, et al., Energy transfer in solid solutions $Zn_xMg_{1-x}WO_4$, Opt. Mater. 36 (2014) 1660–1664.

[4] I.A. Tupitsyna, P.O. Maksimchuk, A.G. Yakubovskaya, et al., Abnormal enhancement of light output by cation mixing in $Zn_xMg_{1-x}WO_4$ nanocrystals, Met. Funct. Mater. 24 (2017) 16–20.

[5] N. Krutyak, V. Nagirnyi, D. Spassky, et al., Luminescent and structural properties of $Zn_xMg_{1-x}WO_4$ mixed crystals, Radiat. Meas. 90 (2016) 43–46.

[6] A. Belsky, A. Gektin, S. Gridin, A.N. Vasil'ev, Electronic and optical properties of scintillators based on mixed ionic crystals, in: M. Korzhik, A. Gektin (Eds.), Springer Proceedings in Physics, vol. 200, 2017, pp. 63–82.

[7] O. Voloshyna, O. Sidletskiy, D. Spassky, et al., Nonlinear behavior of structural and luminescent properties in $Gd(Nb_xTa_{1-x})O_4$ mixed crystals, Opt. Mater. 76 (2018) 382–387.

[8] D. Spassky, A. Vasil'ev, S. Vielhauer, et al., Composition effect in luminescence properties of $Y(Nb_xTa_{1-x})O_4$ mixed crystals, Opt. Mater. 80 (2018) 247–252.

[9] J. Ueda, P. Dorenbos, A.J.J. Bos, K. Kuroishia, S. Tanabe, Control of electron transfer between Ce^{3+} and Cr^{3+} in the $Y_3Al_{5-x}Ga_xO_{12}$ host via conduction band engineering, J. Mater. Chem. C 3 (2015) 5642–5651.

[10] S. Stoll, A. Schweiger, EasySpin, a comprehensive software package for spectral simulation and analysis in EPR, J. Magn. Reson. 178 (2006) 42–55.

[11] M.L. Meilman, M.I. Samoilovich, Vvedenie V Spektroskopiju EPR Aktivirovannych Kristallov, Atomizdat, Moskva, (1977), pp. 126–130.

[12] A.A. Ryadun, E.N. Galashov, V.A. Nadolinny, V.N. Shlegel, ESR and luminescence of $ZnWO_4$ crystals activated by gadolinium ions, J. Struct. Chem. 53 (2012) 685–689.

[13] S.A. Altshuler, B.M. Kozyrev, Electron Paramagnetic Resonance in Compounds of Transition Elements, second ed., John Wiley&Sons Inc., New York, 1974.

[14] Ch.P. Poole, Jr.H.A. Farach (Eds.), Handbook of Electron Spin Resonance, Springer-Verlag, New York, 1999.

[15] A.A. Galkin, G.N. Neilo, G.A. Tsintsad, EPR spectrum of Mn^{2+} in $ZnWO_4$, soviet physics solid state, USSR 9 (1967) 275.

[16] A.I. Zvyagin, V.A. Moiseev, A.M. Pshisukh, EPR of Mn^{2+} in system $ZnWO_4$-$MnWO_4$, soviet physics solid state, USSR 10 (1969) 2046.

[17] Ch.-Ch. Ding, Sh.-Yi Wu, Qi.-Sh. Zhu, et al., Theory studies of the local lattice distortions and the EPR parameters for Cu^{2+}, Mn^{2+} and Fe^{3+} centres in $ZnWO_4$, Mol. Phys. 113 (2015) 1478–1484.

[18] Z. Šroubek, K. Žďánský, Electron spin resonance of Cu^{2+} ion in $CdWO_4$, $ZnWO_4$ and $MgWO_4$ single crystals, J. Chem. Phys. 44 (1966) 3078.

[19] V.V. Laguta, M. Buryi, J. Rosa, et al., Electron and hole traps in yttrium orthosilicate single crystals: the critical role of Si-unbound oxygen, Phys. Rev. B 90 (1–12) (2014) 064104.

[20] D.A. Spassky, V. Nagirnyi, V.V. Mikhailin, et al., Trap centers in molybdates, Opt. Mater. 35 (2013) 2465–2472.

[21] M. Buryi, D.A. Spassky, J. Hybler, et al., Electron Spin Resonance study of charge trapping in α-$ZnMoO_4$ single crystal scintillator, Opt. Mater. 47 (2015) 244–250.

[22] V.V. Laguta, M. Buryi, M. Nikl, et al., Hole capture in $PbWO_4$:Mo,La(Y) scintillator crystals, Phys. Rev. B 83 (1–5) (2011) 094123.

[23] M. Buryi, P. Bohacek, K. Chernenko, et al., Luminescence and photo-thermally stimulated defect-creation processes in Bi^{3+}-doped single crystals of lead tungstate, Phys. Status Solidi B 253 (2016) 895–910.

[24] O.F. Schirmer, The structure of the paramagnetic lithium center in zinc oxide and beryllium oxide, J. Phys. Chem. Solids 29 (1968) 1407–1429.

[25] A. Watterich, L. Kovács, R. Würz, et al., Electron spin-resonance (ESR) and electron-nuclear double-resonance (ENDOR) study of the self-trapped hole in $ZnWO_4$ single crystals, J. Phys. Condens. Matter 13 (2001) 1595–1607.

[26] D.A. Spassky, N.S. Kozlova, A.P. Kozlova, et al., Study of the defects in $La_3Ta_{0.5}Ga_{5.5}O_{14}$ single crystals, J. Lumin. 180 (2016) 95–102.

[27] M. Nikl, V. Babin, J. Pejchal, et al., The stable Ce^{4+} center: a new tool to optimize Ce-doped oxide scintillators, IEEE Trans. Nucl. Sci. 63 (433–438) (2016) 7412783.

[28] R.D. Shannon, Revised effective ionic radii and systematic studies of interatomic distances in halides and chalcogenides, Acta Crystallogr. A 32 (1976) 751–767.

[29] I. Romet, M. Buryi, G. Corradi, et al., Recombination luminescence and EPR of Mn doped $Li_2B_4O_7$ single Crystals, Opt. Mater. 70 (2017) 184–193.

[30] B.E. Kananen, E.M. Golden, S.A. Basun, et al., Dual role of Sb ions as electron traps and hole traps in photorefractive $Sn_2P_2S_6$ crystals, Opt. Mater. Express 6 (2016) 3992–3999.

[31] A. Watterich, A. Hofstaetter, A. Scharmann, O. Szakacs, Al- and OH-related paramagnetic impurity centres in UV- or x-irradiated $ZnWO_4$ single crystals, J. Phys. Condens. Matter 15 (2003) 7073–7084.

[32] V.B. Kravchenko, Crystal structure of the monoclinic form of magnesium tungstate $MgWO_4$, J. Struct. Chem. 10 (1969) 148–149.

[33] A. Watterich, A. Hofstaetter, O^- - Li_{Zn} centers in Li-doped $ZnWO_4$ single crystals characterized by ESR and ENDOR spectroscopy, Solid State Commun. 105 (1998) 357–362.

[34] J.R. Pilbrow, Transition Ion Electron Paramagnetic Resonance, Clarendon Press, Oxford, 1990.

[35] V.V. Laguta, M. Martini, A. Vedda, et al., Electron traps related to oxygen vacancies in $PbWO_4$, Phys. Rev. B 67 (1–8) (2003) 205102.

[36] V.V. Laguta, J. Rosa, M.I. Zaritskii, et al., Polaronic WO_4^{3-} centres in $PbWO_4$ single crystals, J. Phys. Condens. Matter 10 (1998) 7293–7302.

[37] A. Watterich, L.A. Kappers, O.R. Gilliam, Impurity Sn-related paramagnetic defects in UV-illuminated $ZnWO_4$ single crystals, J. Phys. Condens. Matter 11 (1999) 1333–1340.

[38] A. Watterich, A. Hofstaetter, R. Wuerz, et al., Mo^{5+}–H and W^{5+}–H centres in $ZnWO_4$ single crystals characterized by ESR and ENDOR spectroscopy, J. Phys. Condens. Matter 10 (1998) 205–213.

[39] A. Watterich, O.R. Gilliam, L.A. Kappers, K. Raksanyi, ESR of W^{5+} - H centers in γ- or UV-irradiated $ZnWO_4$ single crystals doped by Li, Solid State Commun. 97 (1996) 477–480.

[40] M.I.N. Fujita, Y. Inabe, X-ray photoelectron spectroscopy and electronic structures of scheelite- and wolframite-type tungstate crystals, J. Phys. Soc. Jpn. 75 (1–8) (2006) 084705.

[41] M. Daturi, G. Busca, M.M. Borel, et al., Vibrational and XRD study of the system $CdWO_4$-$CdMoO_4$, J. Phys. Chem. B 101 (1997) 4358–4369.

[42] V. Mürk, M. Nikl, E. Mihokova, K. Nitsch, A study of electron excitations in $CaWO_4$ and $PbWO_4$ single crystals, J. Phys. Condens. Matter 9 (1997) 249–256.

[43] D.A. Spassky, N.S. Kozlova, V. Nagirnyi, et al., Excitation energy transfer to luminescence centers in $M^{II}MoO_4$ (M^{II} = Ca, Sr, Zn, Pb) and Li_2MoO_4, J. Lumin. 186 (2017) 229–237.

[44] A.E. Ovechkin, V.D. Ryzhikov, G. Tamulaitis, A. Žukauskas, Phys. Status Solid A 103 (1987) 285–290.

[45] V. Nagirnyi, L. Jonsson, M. Kirm, et al., Luminescence study of pure and Fe- or Mo-doped $ZnWO_4$ crystals, Radiat. Meas. 38 (2004) 519–522.

[46] M. Itoh, T. Katagiri, T. Aoki, M. Fujita, Photo-stimulated luminescence and photo-induced infrared absorption in $ZnWO_4$, Radiat. Meas. 42 (2007) 545–548.

[47] F. Urbach, The long-wavelength edge of photographic sensitivity and of the electronic absorption of solids, Phys. Rev. 92 (1953) 1324.

[48] K.S. Song, R.T. Williams, Self-Trapped Excitons, second ed., Springer-Verlag, Berlin, 1996.

[49] V.N. Kolobanov, I.A. Kamenskikh, V.V. Mikhailin, et al., Optical and luminescent properties of anisotropic tungstate crystals, Nucl. Instrum. Methods A 486 (2002) 496–503.

[50] V.V. Mikhailin, A.N. Vasil'ev, Introduction to Solid-State Spectroscopy, MGU, Moscow, 1987.

[51] A. Kotlov, L. Jönsson, M. Kirm, et al., Luminescence study of self-trapped holes in pure and Fe or Mo doped $ZnWO_4$ crystals, Radiat. Meas. 38 (2004) 715–718.

[52] N.R. Krutyak, D.A. Spassky, I.A. Tupitsyna, A.M. Dubovik, Influence of peculiarities of electronic excitation relaxation on luminescent properties of $MgWO_4$, Opt Spectrosc. 121 (2016) 45–51.